Variability of 5f states in plutonium carbides

2007 J. Phys.: Condens. Matter 19 476201

(http://iopscience.iop.org/0953-8984/19/47/476201)

J. Phys.: Condens. Matter **19** (2007) 476201 (11pp) doi:10.1088/0953-8984/19/47/476201

Variability of 5f states in plutonium carbides

T Gouder[1], L Havela[2], A B Shick[3], F Huber[1], F Wastin[1] and J Rebizant[1]

[1] European Commission, Joint Research Centre, Institute for Transuranium Elements, Postfach 2340, 76125 Karlsruhe, Germany
[2] Faculty of Mathematics and Physics, Department of Condensed Matter Physics, Charles University, Ke Karlovu 5, 121 16 Prague 2, Czech Republic
[3] Institute of Physics, Academy of Sciences of the Czech Republic, 182 21 Prague 8, Czech Republic

E-mail: havela@mag.mff.cuni.cz

Received 23 July 2007, in final form 2 October 2007
Published 31 October 2007
Online at stacks.iop.org/JPhysCM/19/476201

Abstract

Valence-band photoelectron spectra of Pu_2C_3 and $PuC_{0.85}$ reveal the same type of 5f features below the Fermi level as observed for the majority of other Pu systems. They appear at the same energies (0–0.1, 0.5, and 0.85 eV) and their intensity is higher for Pu_2C_3 than for $PuC_{0.85}$. We deduce that they can be attributed to the $5f^5$ final-state multiplet originating in the $5f^6$ component of the ground state. The higher 5f occupancy (5.48), calculated in Pu_2C_3, explains its non-magnetic character.

(Some figures in this article are in colour only in the electronic version)

1. Introduction

Three Pu carbides are known to be thermodynamically stable at room temperature. Besides Pu_3C_2 with structure and other characteristics unknown, there is PuC_{1-x}, forming with the NaCl type of structure, and Pu_2C_3, crystallizing in a *bcc* (body-centred cubic) structure [1]. The carbon-deficient Pu monocarbide should contain random anionic vacancies similar to other actinide monocarbides, leading to estimated boundary concentrations $PuC_{0.78}$–$PuC_{0.89}$ [2]. The stoichiometry variations are reflected in various values of the lattice parameter and magnetic ordering temperature [3], but there is no doubt that PuC_{1-x} at the C-rich limit undergoes a magnetic phase transition at ≈100 K, leading to a simple antiferromagnetic structure with Pu moments along the (0, 0, 1) direction [4]. In contrast to that, Pu_2C_3 is paramagnetic, with a susceptibility χ_0 that increases weakly with decreasing temperature T, reaching 0.63×10^{-8} m^3 mol^{-1} (lower than in any of the structure modifications of Pu metal) in the low-T limit. The Pu–Pu spacing, d_{Pu-Pu}, is somewhat higher in the monocarbide (350 pm) than in Pu_2C_3 (336 pm), both being in the range close to the Hill limit (≈340 pm) [5]. This critical spacing separates compounds, in which the large Pu–Pu overlap suppresses the tendency to band magnetism, from those with higher d_{Pu-Pu}, in which magnetic order is possible. Such

a situation as in the Pu carbides can therefore give detailed insight into the reason for the non-magnetic behaviour of certain Pu compounds, while their U and Np counterparts (U_2C_3 and Np_2C_3 in this case) are magnetic [3]. As discussed in [6], besides the variations in d_{Pu-Pu}, there can be a varying strength of 5f-ligand hybridization and/or varying 5f occupancy, which can determine the magnetic character of Pu-based systems. The aim of the present study is to investigate how the basic features of electronic structure, revealed by photoelectron spectroscopy, vary between PuC_{1-x} and Pu_2C_3, and how they correlate with spectra of other non-magnetic Pu systems, such as PuSe, PuTe or δ-Pu.

2. Experimental details

Thin layers of Pu carbides were synthesized *in situ* by sputter co-deposition using the sputter source for microtargets, modified into a two-target setup. High-purity Ar was used as a sputter gas. The stoichiometry was tuned by varying the voltages for the Pu and C targets and monitoring the respective ion currents, varying typically in the range 0.1–10 mA. The setup was analogous to that used previously for depositing U–C layers [7]. The Pu–C ratio was quantified using x-ray photoelectron spectroscopy (XPS, see below). Si wafers cleaned by heating to 673 K and sputtering by Ar ions of 1 keV energy were used as a substrate. The time of sputter deposition (typically 40 s at a deposition rate 0.1 nm s^{-1}) was sufficient to produce layers thick enough to cover the whole information depth of the photoelectron spectroscopy (at least ten monolayers). Varying the temperature of the substrate between 123 and 523 K did not yield any significant differences in photoelectron spectra.

Photoemission data were collected using a spectrometer equipped with a Leybold LHS-10 analyzer, an x-ray source providing Al Kα radiation ($h\nu = 1486.6$ eV) and an ultraviolet (UV) source (HeI and HeII radiation, $h\nu = 21.22$ eV and 40.81 eV, respectively). The Au Fermi edge and Au-$4f_{7/2}$ line were used to calibrate the spectrometer energy. The sputter deposition was carried out in the preparation chamber of the spectrometer and the layers were never exposed to normal atmosphere. All spectra given were corrected for the transmission function of the spectrometer.

3. Results

3.1. X-ray photoelectron spectroscopy

The stoichiometry of the deposited layers was determined by means of XPS, using integrated intensities (subtracting the Shirley background) of Pu-4f and C-1s core-level lines. The values obtained were analysed considering both empirical sensitivity factors and, after correction for the transmission function of the spectrometer, the theoretical photo-ionization cross-section values (both methods are discussed for actinides in [8]). Experience with, for example, actinide nitrides [9] shows that the latter method underestimates the concentration of the light element by about 30%, which is analogous to the present situation with the Pu–C system. Therefore here we give stoichiometries determined on the basis of the empirical sensitivity factors. The relative precision (estimated as 10%) is negatively affected by a very weak intensity of the C-1s line (about 40 times weaker than the $4f_{7/2}$ line used for the comparison).

By varying the deposition currents for the Pu and C targets, we were able to tune the stoichiometries of the deposited layers in a reproducible way between $PuC_{0.50}$ and $PuC_{1.80}$. Figures 1 and 2 demonstrate the concentration variations of the C-1s and Pu-4f lines. At the lowest C concentration, the C-1s line is quite narrow, located at binding energy (BE) of 282.6 eV (marked by the vertical dashed line). Approaching the stoichiometry of the range of

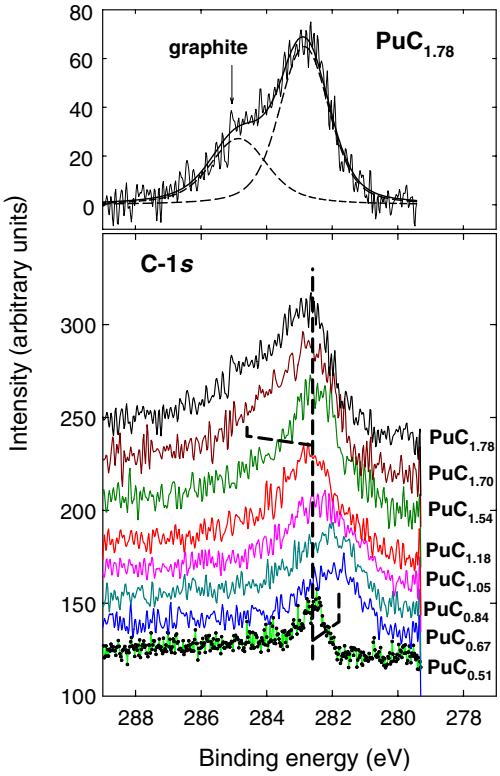

Figure 1. C-1s XPS spectra of Pu–C layers for varying stoichiometry. The dashed line indicates schematically the energy shifts towards lower BE values for lower C concentrations up to approximately PuC and the opposite shift of the spectral weight for higher C concentration. The upper panel demonstrates the second component, attributed to graphite, appearing for very high C concentration. Before decomposition into the two spectral features, the secondary-electron background was subtracted in this case.

stability of PuC_{1-x}, the C-1s line broadens markedly and its centre of weight shifts towards lower binding energies, to approximately 281.5 eV. The broadening can be associated with the structural disorder in the cubic phase due to the C vacancies. With a further increase in the C concentration, the spectral weight is gradually moved back by 1 eV for $PuC_{1.5}$. Increasing the C concentration even more, a second feature develops at a BE of 284.8 eV, which can be attributed to the pure carbon (graphite), known to be manifested at this BE [10].

Figure 2 shows the variations in concentration of the Pu-4f spectra, consisting of the $4f_{5/2}$ and $4f_{7/2}$ doublet split due to the spin–orbit interaction, compared with the spectra of α-Pu and PuN. One can immediately distinguish that in all the Pu–C systems the main spectral response is located at binding energies much higher than the main line in α-Pu (422.2 eV for $4f_{7/2}$, which is the more intense line, with better resolved details for the majority of Pu systems), and it roughly coincides with that of PuN (423.6 eV) [9]. For high Pu concentrations, it is broader than in PuN, which can again be understood as being due to the disorder in the PuC_{1-x} phase. The spectrum corresponding to $PuC_{0.51}$ is broadened even more: one can even suspect the presence of two unresolved, roughly equal features.

The energy of the maximum is in fact a little (by 0.3–423.9 eV) shifted with respect to PuN, and a further shift (to 424.5 eV) is recorded for concentrations around $PuC_{1.50}$ and higher.

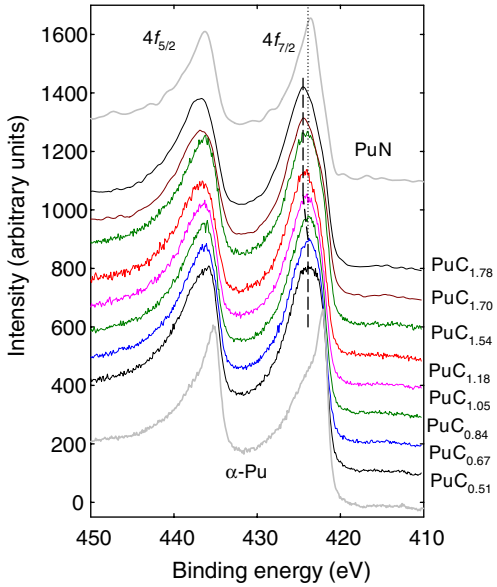

Figure 2. Pu-4f spectra for the same Pu–C concentrations as shown in figure 1, compared with α-Pu (bottom) and PuN (top). The dashed and dotted lines show the shift of the maxima of the $4f_{7/2}$ lines with C concentration.

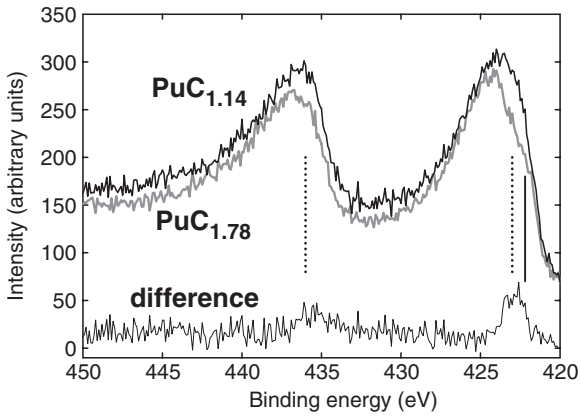

Figure 3. Comparison of Pu-4f spectra obtained for two selected concentrations in a higher-resolution mode. The dotted lines mark the maxima of the difference spectrum, plotted at the bottom. The full line indicates the position of the $4f_{7/2}$ peak for α-Pu.

At the same time, the $4f_{7/2}$ peak becomes noticeably asymmetric. It was discussed in [9] that the shift of the 5f lines towards higher BE values (with respect to the pure actinide metal) depends on the ionicity of the compound and the hybridization of the 5f states with the electronic states of ligands. In this framework, the Pu carbides follow a similar pattern as is found in actinide nitrides, with higher nitrides exhibiting an even larger BE shift than the mononitrides [9]. (Pu does not form any higher nitride, but this tendency was observed for U and Th [9].)

To distinguish better the real shape of the 4f emission, we performed additional scans with enhanced energy resolution ($\approx$1.0 eV compared to $\approx$1.3 eV for the standard setting). The results are shown in figure 3. The shape, especially of the $4f_{7/2}$ peak in the C-rich Pu–C, is

clearly indicative of two poorly resolved features, with the weaker one, approximately at the energy of the α-Pu peak (shown by a full line), forming a pronounced shoulder on the low-BE side of the more intense feature.

Comparing the results on sputter deposited films with the equilibrium phase diagram, one has to bear in mind that the product of sputter deposition can be far from thermodynamic equilibrium. In particular, the deposited material can accommodate much broader off-stoichiometry in the form of lattice imperfections and, for certain stoichiometries, the expected phase separation may be hindered. Consequently, there is, in general, uncertainty about the correspondence to the phases known from the Pu–C phase diagram. In the present study, the high-C part of our system is relatively well defined. The fact that pure graphitic carbon segregates if the C concentration exceeds $PuC_{1.5}$ is strongly suggestive that Pu_2C_3 is indeed the last (under the conditions used) C-rich phase that can be obtained. Although the C-deficient PuC does not form congruently, its high temperature of formation ($\approx$1650 °C) indicates its high stability, and we may also expect that it will form during the sputter deposition process in the proper cubic structure, at least in the concentration range given by the phase diagram, or perhaps encompassing a broader concentration range, similarly to UN [11] or US [12]. This corresponds to the range where both the C-1s and Pu-4f spectra are fixed at particular energies, but broadened due to the lattice disorder.

The least information can be deduced about the Pu-rich part. Although the $PuC_{0.51}$ data could correspond to the Pu_3C_2 bulk phase, the fact that this phase forms only below 575 °C suggests a low enthalpy of mixing and then a low probability of forming. Alternatively, we may speculate about C diluted in some of the Pu phases or strongly under-stoichiometric PuC. Due to the poor definition of the material that is studied, this part of the phase diagram was not included in further study using UPS.

Due to the difficult handling of transuranium materials, no structural studies using x-ray diffraction have been undertaken. Crystallinity of the deposited phases has to be expected, especially for deposition on a heated substrate, on the basis of comparison with detailed structure studies of UN, U_2N_3 [11] and US [12]. The most direct analogy can be drawn with U–C compounds prepared under practically identical conditions [7]. While the crystal-structure parameters of the sputter-deposited material (such as residual strain, microstrain, texture) differ from a conventional bulk material of the same composition, photoelectron spectroscopy as a typical local-probe technique is rather insensitive to such details.

3.2. Valence-band UPS

Ultraviolet photoelectron (UPS) studies using two different photon energies (HeI, 21.22 eV, and HeII, 40.81 eV) can distinguish the emission from the 5f states. The important fact is that, while the 5f photoexcitation cross section is negligible for HeI, it is strongly enhanced in HeII, which makes the 5f emission dominate the valence-band spectra. Figure 4 displays the HeI and HeII spectra of $PuC_{0.85}$ and $PuC_{1.51}$, denoted as PuC_{1-x} and Pu_2C_3, respectively. While $PuC_{0.85}$ is representative of the whole concentration range from $PuC_{0.81}$ to $PuC_{1.12}$ (here the differences are negligible), the spectra of Pu_2C_3 also represent well all materials with still higher C concentration.

As in most of other Pu systems [6, 9, 13, 14], the HeII spectra are characterized by the fingerprint of a triplet of sharp features, located at (or slightly below) the Fermi energy E_F (feature A), and at 0.50 (B) and 0.85 eV (C) BE. The last one seems to be slightly shifted closer to E_F (to 0.80 eV) for $PuC_{0.85}$. Although the 5f character in all three features clearly dominates, the Fermi level is also well distinguished for the HeI spectra, suggesting a non-negligible non-f contribution in analogy to the situation in Pu metal. In addition, we have to

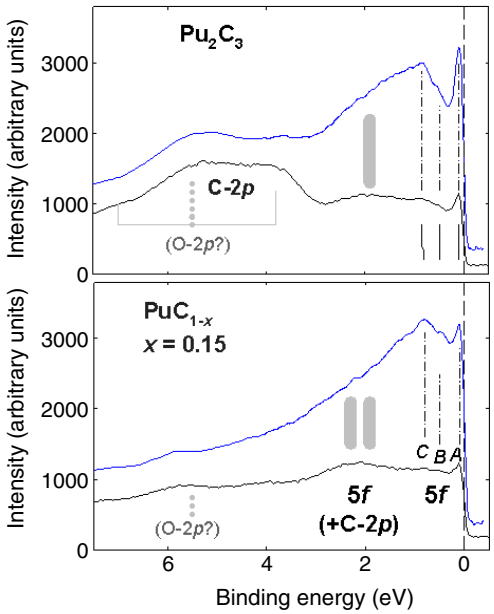

Figure 4. UPS valence-band spectra for the HeI (black or bottom) and HeII (blue or top) photoexcitation for two films, identified as belonging to pure phases $PuC_{0.85}$ and Pu_2C_3. The dash–dotted lines indicate energies of the triplet of lines (mostly) of the 5f type of emission.

assume a 5f intensity in the energy range around 2 eV BE, overlapping perhaps (as the variations in cross section with photon energy suggest) with the C-2p states. In HeII, this emission is more pronounced, forming a shoulder to the peak *C* in Pu_2C_3. It is less noticeable for PuC_{1-x}, which may be due to a higher contribution of C-2p, or due to a certain shift of the 5f intensity in this range towards E_F. The emission from the C states may be compared to the U–C system [7], in which the C-2p emission (not overlapping with the 5f states) appears at 2.5 eV for $UC_{0.8}$, whereas it is displaced to 6 eV for C concentrations from $UC_{1.3}$ upwards. In Pu_2C_3, the C-2p states clearly dominate the spectra at higher BE, from 4 eV onwards, which is also the energy range of the 2p emission in graphitic C [10]. Therefore we cannot decide if a small amount of graphite, possibly segregated at the surface due to its excess over the Pu_2C_3 stoichiometry, also contributes in this energy range. Any small O contamination can also show up as the O-2p emission at 5.5 eV, visible both in HeI and HeII, but the fact that the Pu–C layers around the 1:1 stoichiometry are practically O-free does not leave much space for any O contamination to be present in Pu_2C_3.

4. Discussion and electronic-structure calculations

The observed valence-band spectra of both Pu carbides are similar to most of the Pu-based metallic systems studied so far. Although the intensities may vary, the triplet within 1 eV below E_F is observable for most clean (i.e. oxygen-free) surfaces. Only PuSb, with presumably a well-defined $5f^5$ localized ground state (for which the 5f emission in this energy range is practically absent [13, 15]), and α-Pu [16] (which can be considered as a 5f band system), represent two exceptions. Because the binding energies of the triplet lines are practically invariable (while their intensity can vary strongly and they dominate the valence-band spectra

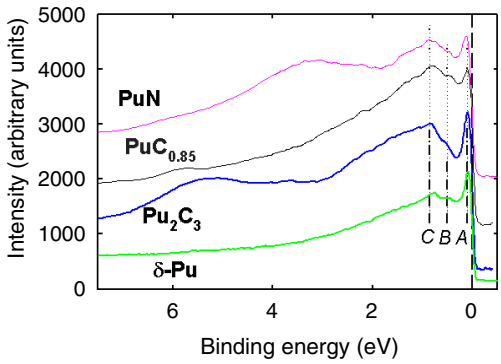

Figure 5. Comparison of the HeII UPS spectra for the two Pu carbides from figure 4 with δ-Pu and PuN. The thick vertical bar indicates an approximate energy position of further 5f emission in $PuC_{0.85}$ and Pu_2C_3.

in PuSe [15] and PuTe [13]), it was recognized [9, 15] that they cannot be associated with any particular energy bands. Instead, multiplet excitations belonging to a final state, or many-body effects, were considered as plausible general mechanisms responsible for the three lines. Although a simple comparison with the calculated 5f atomic spectra [17] reveals a conspicuous similarity, only recent Hubbard I (HIA) calculations [18], connecting the atomic correlations with the underlying electronic structure of the crystalline solid, demonstrated that the calculated energies and intensities of the $5f^5$ final-state multiplet lines correspond to the observed features in δ-Pu. The LDA + U 'around mean field' calculations of the ground state, which serves as the basis for Hubbard I, leads to an 5f occupancy higher than 5.0 ($n_f = 5.44$ in pure δ-Pu [19]), and it is therefore the admixture of the $5f^6$ component into the $5f^5$ ground state which gives rise to the final-state $5f^5$ multiplet. Following the suggestion that the $5f^6$ component suppresses magnetism in Pu compounds (appearing for the $5f^5$ ground state) [6], it is tempting to relate the more intense triplet features in Pu_2C_3 compared to those in $PuC_{0.85}$ (based on the intensity of the feature at E_F) to a higher 5f occupancy in the former case, which would be responsible for the non-magnetic character of Pu_2C_3. It is also interesting to point out a closer similarity of Pu_2C_3 and δ-Pu (both non-magnetic) HeII spectra seen in figure 5, whereas $PuC_{0.85}$ resembles more the PuN (magnetically ordered) spectrum [9].

To examine the 5f occupancy (n_f), we performed the LDA + U calculation for PuC, representing for simplicity $PuC_{0.85}$ (with a lattice parameter of 9.414 bohr) and Pu_2C_3. For PuC, we considered various types of magnetic ground state: ferromagnetic (FM) structure, simple antiferromagnetic structure with moments along (0, 0, 1) (AFM, deduced from experiment), and the forced non-magnetic (NM) state making use of two different flavours of the LSDA + U method, namely the around-mean-field (AMF) and the fully localized limit (FLL) forms of double counting (see [19] and references therein for further details).

The LSDA + U calculations of PuC always yield an FM state lower in total energy than the forced NM state, indicating the formation of a local magnetic moment on the Pu atom, with a calculated total energy gain (due to the moment formation) of 74 mRyd (FLL) and 46 mRyd (AMF) per unit cell. While for both the forced NM-AMF and NM-FLL states the $n_f = 5.23$ counts are practically the same, the AMF-FM yields $n_f = 5.11$ and the FLL-FM $n_f = 4.99$. The values of the Pu spin (M_S), orbital (M_L) and total (M_J) magnetic moments strongly depend on the choice of the type of double counting (see table 1). The n_f count and magnetic moments are practically equal in the FM and AFM magnetic states. The resulting FLL values, $M_J = 0.8$–$0.9\ \mu_B$, are compatible with the estimate based on neutron diffraction

Table 1. Calculated occupation of the 5f-manifold (n_f), local spin (M_S), orbital (M_L) and total (M_J) magnetic moments (in μ_B) for an Pu atom, assuming different types of magnetic states (FM—ferromagnetic, AFM—antiferromagnetic, NM—non-magnetic) and different types of LDA + U double counting (AMF—'around mean field', FLL—'fully localized' limits) in PuC and Pu_2C_3.

	n_f	M_S	M_L	M_J
	PuC			
FM-FLL-LDA + U	4.99	−2.99	3.79	0.80
FM-AMF-LDA + U	5.11	−0.60	2.32	1.72
AFM-FLL-LDA + U	4.97	−2.82	3.71	0.89
AFM-AMF-LDA + U	5.11	−0.61	2.45	1.84
NM-FLL-LDA + U	5.23	0	0	0
NM-AMF-LDA + U	5.23	0	0	0
	Pu_2C_3			
AMF-LDA + U	5.48	0	0	0

data (0.7–0.8 μ_B [4]), whereas the values for the 'around mean field' calculation, $M_J \approx 1.7\ \mu_B$, are too large.

The total and f-projected LDA + U densities of states (DOS) and LDA + HIA spectral densities (SD) for PuC are shown in figure 6(a). The Hubbard I approximation used here is based only on excitation within the Pu-5f manifold, capturing the $5f^n \rightarrow 5f^{n-1}$ processes. Not included remain the interaction of the non-f electrons with the photohole (conduction-electron screening processes) as well the f-electron screening ($5f^n \rightarrow 5f^n$ processes), which can contribute if some itinerancy of the 5f states is preserved. The calculated spectral densities do not include photoexcitation matrix elements, which can in general be energy dependent. Nevertheless, the 5f cross section dominates for the photon energies over 40 eV for actinide atoms [20]. This, together with the fact that the calculated features correspond to quasi-intra-atomic excitations including the f-states, gives a justification for using the calculated spectral density for a semi-quantitative analysis of the valence-band spectra.

A comparison with the experimental UPS spectra shows that the LDA + U DOS does not describe correctly the experimental photoelectron spectra of PuC—a large part of the f-manifold is wrongly located in the 2–4 eV binding energy range. When the multiplet transitions are included with the help of LDA + HIA, the f-manifold is correctly shifted towards E_F. Still, LDA + HIA fails to describe fully the experimental PES, and no peak is found at E_F. In fact, the absence of the peak is directly related to the f^5 character of the calculated PuC ground state obtained in the calculations.

Assuming that the calculated value $n_{5f} \approx 5.0$ cannot be far from reality, we can ascribe the inconsistency to the insufficiency of HIA to describe fully the photoemission process mentioned above. Besides that, there is an insufficiency of LDA + HIA in the description of many-body physics, leading to heavy quasi-particles. This means that, although no multiplet transition appears at the Fermi level, the experimentally observed peak can be due to many-body physics, remaining beyond the framework of LDA + HIA [18]. Besides these fundamental reasons, the difference between the observed and calculated spectral densities can also be due simply to the vacancies in the C sublattice (not considered in the calculations), which could eventually shift the 5f charge balance.

For Pu_2C_3, the situation is different. The FLL-LDA + U calculation always yields a strongly magnetic state, in contradiction to the experimentally observed paramagnetic ground state. On the contrary, the AMF-LDA + U yields practically zero magnetic moments on Pu atoms, and $n_f = 5.48$. The increase in f-count is mostly complemented by the decrease in

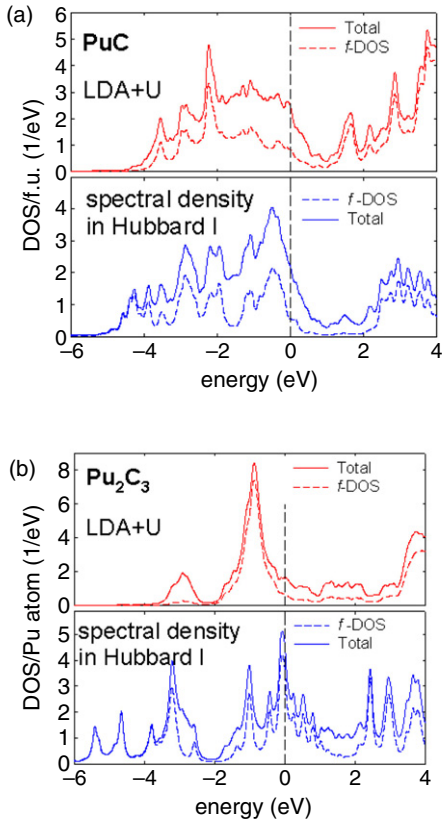

Figure 6. Density of states and spectral density (total—full line, f-projected—dashed line) for (a) PuC (FLL-LDA + U, real antiferromagnetic structure) and (b) Pu_2C_3 (AMF-LDA + U). The vertical dashed line indicates the Fermi level.

the occupation of the Pu-6d states by about 0.4/Pu. We note that all calculations assume a collinear spin M_S magnetic moment alignment. However, since the crystal structure of Pu_2C_3 is non-centrosymmetric, various non-collinear structures could in principle develop; these are left for further consideration.

In figure 6(b) we show the LDA + U DOS and HIA spectral density. LDA + U gives most of the Pu-5f DOS at around 1 eV binding energy. At variance with PuC, there are non-f-states (mostly the p-states of carbon) in the region 3–5 eV, in qualitative agreement with the UPS spectra shown in figure 4. When the multiplet transitions are included by means of LDA + HIA, the universal A, B, and C peaks appear at binding energies of 0.08, 0.44, and 1.01 eV. These features are consistent, within the expected accuracy, with the observed UPS spectra shown in figure 4. In contrast to the experiment, the calculations yield practically no f-state shoulder at around 2 eV in binding energy. With an increase in binding energy, there are predominantly C-2p states together with 5f emission due to unresolved $f^5 \rightarrow f^4$ multiplet-transition lines at energies up to 8 eV, in agreement with the UPS spectra of figure 4. Here we assume that the lifetime broadening due to the limited lifetime of the photohole smears details progressively with increasing BE.

The fact that Pu_2C_3 with a 5f occupancy clearly exceeding 5.0 is better described by the AMF-LDA + U calculations, while PuC with an occupancy close to 5.0 is better described by

the FLL-LDA + U, does not need to be purely accidental. This can be understood as follows: different flavours of LDA + U, namely AMF and FLL, represent different constraints. In the case of FLL-LDA + U, one variationally searches for a f-manifold solution that is as close as possible to the single Slater determinant state with integer local occupations in an atomic-like localized basis. Hereby FLL-type double counting has an advantage in the situation close to 5f integral occupancy and is better suited to the $5f^5$ configuration of PuC.

Instead, in the case of AMF-LDA + U, the variational minimization drives the solution to the single Slater determinant in a Bloch wave band-like basis, allowing non-integer local occupations of the f-manifold. This method is therefore suitable for describing the solution which consists of a superposition of $5f^5$ and $5f^6$ single determinant states. This is why the mixed-valence 5f-manifold with $n_f = 5.48$ is better suited to Pu_2C_3 and is quite analogous to δ-Pu [18, 19].

Here it must be stressed that the non-magnetic character of such Pu systems is not due to a close proximity to the non-magnetic $5f^6$ state, as misinterpreted for the LDA + U calculations of δ-Pu in [21]. The LDA + U method, complemented by HIA, provides such a level of electronic-structure description that the suppression of magnetism is correctly captured for the 5f occupancy below $\approx$5.5, while the high spectral density at the Fermi level explains the enhancement of the electronic specific heat and other quantities related to the strongly correlated nature.

5. Concluding remarks

We have shown that LDA + U calculations can describe correctly the variations in magnetic properties between PuC_{1-x} and Pu_2C_3. The main difference consists of the partial occupancy of the $5f^6$ states in the latter compound. Supplemented by Hubbard I calculations of spectral density, the calculations qualitatively explain the dominant features of photoelectron spectra as related to $5f^5$ and $5f^4$ final-state multiplets, which proves the strongly correlated character of the Pu-5f states. Hereby it provides a better understanding of a broad class of Pu compounds, describing within a uniform theoretical approach (without free parameters) photoelectron spectra as well as the type of ground state and the size of magnetic moments.

Acknowledgments

This work is part of the research plan MSM 0021620834 financed by the Ministry of Education of the Czech Republic. It was also supported by the Grant Agency of the Academy of Sciences under grant IAA100100530. Participation in the European Commission JRC-ITU Actinide User Laboratory program through the support of the European Community-Access to Research Infrastructures action of the Improving Human Potential Programme (IHP), contract RITA-CT-2006-026176, is acknowledged. Authors are indebted to V Drchal for fruitful discussion of the theoretical aspects. The high-purity Pu metal required for the fabrication of the compounds was made available through a loan agreement between the Lawrence Livermore National Laboratory (LLNL) in the USA and the Institute for Transuranium Elements (ITU), in the frame of a collaboration involving LLNL, Los Alamos National Laboratory, and the US Department of Energy.

References

[1] Mulford R N R, Ellinger F H, Hendrix G S and Albrecht E D 1961 *Plutonium 1960* (London: Cleaver-Hume Press) pp 301–11

[2] Manes L and Benedict U 1985 *Actinides—Chemistry and Physical Properties* ed L Manes (Berlin: Springer) pp 77–126

[3] Lam D J and Aldred A T 1974 *The Actinides: Electronic Structure and Related Properties* vol I, ed A J Freeman and J B Darby Jr (New York: Academic) pp 109–79
[4] Green J L, Arnold G P, Leary J A and Nereson N G 1970 *J. Nucl. Mater.* **34** 281
[5] Hunter Hill H 1970 *Plutonium 1970 and Other Actinides* ed W N Miner (AIME) pp 2–19
[6] Havela L, Javorsky P, Wastin F, Colineau E, Gouder T, Shick A B and Drchal V 2007 *J. Alloys Compounds* **444–445** 88
[7] Eckle M, Eloirdi R, Gouder T, Colarieti-Tosti M, Wastin F and Rebizant J 2004 *J. Nucl. Mater.* **334** 1
[8] Gouder T and Havela L 2002 *Microchim. Acta* **138** 207
[9] Havela L, Wastin F, Rebizant J and Gouder T 2003 *Phys. Rev.* B **68** 085101
[10] Bachman B J and Vasile M J 1989 *J. Vac. Sci. Technol.* A **7** 2709
[11] Rafaja D, Havela L, Kuzel R, Wastin F, Colineau E and Gouder T 2005 *J. Alloys Compounds* **386** 87
[12] Havela L, Miliyanchuk K, Rafaja D, Gouder T and Wastin F 2006 *J. Alloys Compounds* **408–412** 1320
[13] Durakiewicz T, Joyce J J, Lander G H, Olson C G, Butterfield M T, Guziewicz E, Arko A J, Morales L, Rebizant J, Mattenberger K and Vogt O 2004 *Phys. Rev.* B **70** 205103
[14] Joyce J J, Wills J M, Durakiewicz T, Butterfield M T, Guziewicz E, Sarrao J L, Morales L A, Arko A J and Eriksson O 2003 *Phys. Rev. Lett.* **91** 176401
[15] Gouder T, Wastin F, Rebizant J and Havela L 2000 *Phys. Rev. Lett.* **84** 3378
[16] Havela L, Gouder T, Wastin F and Rebizant J 2002 *Phys. Rev.* B **65** 235118
[17] Gouder T, Eloirdi R, Rebizant J, Boulet P and Huber F 2005 *Phys. Rev.* B **71** 165101
[18] Shick A, Kolorenč J, Havela L, Drchal V and Gouder T 2007 *EPL* **77** 17003
[19] Shick A B, Drchal V and Havela L 2005 *Europhys. Lett.* **69** 588
[20] Yeh J J and Lindau I 1985 *At. Data Nucl. Data Tables* **32** 1
[21] Pourovskii L V, Kotliar G, Katsnelson M I and Lichtenstein A I 2007 *Phys. Rev.* B **75** 135107